Defects in Heavy-Fermion Materials: Unveiling Strong Correlations in Real Space

Jeremy Figgins and Dirk K. Morr
Department of Physics, University of Illinois at Chicago, Chicago, IL 60607, USA
(Dated: January 21, 2010)

Complexity in materials often arises from competing interactions at the atomic length scale. One such example are the strongly correlated heavy-fermion materials where the competition[1] between Kondo screening[2] and antiferromagnetic ordering is believed to be the origin of their puzzling non-Fermi-liquid properties[3–8]. Insight into such complex physical behavior in strongly correlated electron systems can be gained by impurity doping[9–12]. Here, we develop a microscopic theoretical framework to demonstrate that defects implanted in heavy-fermion materials provide an opportunity for unveiling competing interactions and their correlations in real space. Defect-induced perturbations in the electronic and magnetic correlations possess characteristically different spatial patterns that can be visualized via their spectroscopic signatures in the local density of states or non-local spin susceptibility. These real space patterns provide insight into the complex electronic structure of heavy-fermion materials, the light or heavy character of the perturbed states, and the hybridization between them. The strongly correlated nature of these materials also manifests itself in highly non-linear quantum interference effects between defects that can drive the system through a first-order phase transition to a novel inhomogeneous ground state.

The essential features of heavy fermion materials is a Kondo lattice of magnetic atoms with localized moments arising from $4f$ or $5f$-electron shells, and a delocalized conduction band[13]. The magnetic moments are coupled to each other via an antiferromagnetic interaction, $I > 0$, and to the spin moments of the conduction electrons via the Kondo coupling, $J > 0$[1,2]. The ground state of this system is realized either by Kondo screening of the magnetic moments, resulting in a heavy-Fermi-liquid phase[13], or by their antiferromagnetic ordering. These two competing phases, which manifest strongly correlated many-body states, are separated by a quantum critical point (QCP). To date, no theoretical consensus has been reached[14–19] on the physical origin for the astonishing deviations from Landau's Fermi-liquid theory observed in the quantum critical region above the QCP[3–8]. Understanding how the formation of antiferromagnetism competes locally with the creation of a Kondo singlet, how coherence is established in Kondo lattices, and how the resulting magnetic and electronic correlations are intertwined, is crucial in unraveling this mystery.

By their very nature defects implanted in a Kondo lattice[20–23] manifest local perturbations that can reveal the form of strong correlations in real space. These defects can take the form of missing magnetic Kondo atoms, i.e., Kondo holes, or of non-magnetic impurities. By differently perturbing the electronic and magnetic states of the system, defects provide an unprecedented opportunity to differentiate (in real space) between electronic correlations arising from Kondo screening, and the antiferromagnetic correlations between the magnetic moments, as schematically shown in Fig. S1 of the Supplementary Information. The spatial form and extent of these perturbations are not only a measure for the strength of the correlations, but also provide insight into the hybridization of the (heavy) magnetic f-electron states with the (light) conduction band. This hybridization results in the Kondo screening of the magnetic moments and the opening of a gap in the electronic spectrum. The experimentally accessible, spectroscopic fingerprints of the perturbed electronic and magnetic correlations can be found in a redistribution of spectral weight in the local density of states of the conduction band, and in an enhancement or suppression of the f-electron spin susceptibility, respectively. Modulations in the density of the conduction electrons, as induced by a non-magnetic impurity, have profound effects on the spatial form of the correlations, and lead to the formation of an impurity bound inside the hybridization gap. The coupling between electronic and magnetic correlations can create highly non-linear feedback effects on quantum interference in periodic arrays of Kondo holes, leading to the spatial reconstruction of the ground state via a first order phase transition. Our findings open a new path for studying competing interactions in real space, and provide a microscopic, real space picture of the perturbations induced by defects in heavy fermion materials.

In order to study the spatial perturbations induced by defects in the magnetic and electronic correlations of a (heavy fermion) Kondo lattice system, we have developed a real-space formalism, the *Kondo-Bogoliubov-de Gennes method*, whose details are described in Sec. S2 of the Supplementary Information. This theoretical formalism provides us with two salient quantities that determine the physical properties of the system. The first one is the site-dependent hybridization, $s(\mathbf{r})$, between the conduction band and the f-electron state of a Kondo atom. It is a measure of the Kondo screening of the magnetic moment, and of the electronic correlations in the resulting many-body state. Here, we focus on the Kondo screened phase of the heavy-fermion materials where $s(\mathbf{r}) \neq 0$ for all sites. The second quantity, $\chi(\mathbf{r}, \mathbf{r}')$, represents the

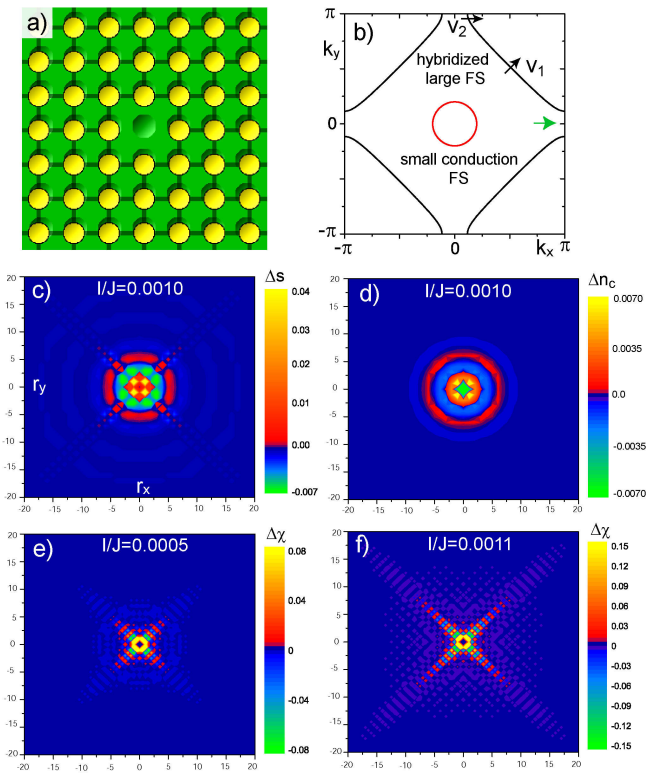

Figure 1: **A hole in the Kondo lattice a.** Schematic picture of a Kondo lattice containing a Kondo hole: green (orange) dots represent the sites of the conduction lattice (magnetic atoms). **b.** Electronic Structure of an unperturbed Kondo lattice system for $I/J = 0.001$: the large Fermi surface (black) arises from the hybridization of the magnetic f-electron states with the conduction band, the small Fermi surface (red) represents the (unhybridized) conduction band. Spatial contour plots of **c.** Δs and **d.** Δn_c for $I/J = 0.001$. Spatial contour plots of $\Delta\chi$ for **e.** $I/J = 0.0005$, and **f.** $I/J = 0.0011$. The relative changes, Δs, Δn_c, and $\Delta\chi$, are obtained by subtracting the results for $s(\mathbf{r})$, $n_c(\mathbf{r})$ and $\chi(\mathbf{r},\mathbf{r}')$ in the unperturbed Kondo lattice from those of the Kondo hole system, and dividing by the former. We display the value of $\chi(\mathbf{r},\mathbf{r}')$ between nearest neighbor sites $\mathbf{r}$ and $\mathbf{r}'$ at $(\mathbf{r}+\mathbf{r}')/2$.

strength of short-range antiferromagnetic correlations between magnetic moments on (nearest-neighbor) sites $\mathbf{r}$ and $\mathbf{r}'$[18,19].

The simplest defect in a Kondo lattice is realized by removing a magnetic Kondo atom from it, resulting in a Kondo hole, as shown in Fig. 1a. To demonstrate the spatial perturbations in the electronic and magnetic correlations of the system that are induced by the Kondo hole, we present in Figs. 1c and 1d, a two-dimensional contour plot of the relative change in the hybridization, Δs, and the conduction electron density, Δn_c, respectively, between the Kondo lattice with and without a hole. Both quantities exhibit similar spatial oscillations, whose isotropy and wavelength of $5a_0$ (a_0 being the lattice constant) imply that they are determined by the Fermi surface of the unhybridized conduction band (see Fig. 1b) with Fermi wavelength $\lambda_F^c = 10a_0$. These oscillations decay exponentially but remain practically unchanged over the range of I/J considered here. The spatial plots of $\Delta\chi$ in Figs. 1e and 1f reveal strongly anisotropic oscillations along the lattice diagonal. Their weaker reflection can also be found in Δs (see Fig. 1c), clearly demonstrating the coupling between the system's electronic and magnetic correlations. The spatial pattern of $\Delta\chi$ is determined by the strongly anisotropic Fermi surface of the hybridized system, shown in Fig. 1b, which possesses a large degree of nesting and a Fermi velocity, v_1, along the lattice diagonal which is about 10 times larger than that along the bond direction, v_2. This conclusion receives further support from the rapid oscillations in $\Delta\chi$ along the lattice diagonal (see Fig. S2 in the Supplementary Information) which possess a wavelength of $\lambda_F^f/2 = \sqrt{2}a_0$, with λ_F^f being the Fermi wavelength of the hybridized Fermi surface along the diagonal. The envelope of these oscillations decays exponentially with distance, r, from the Kondo hole, i.e., $\Delta\chi \propto \exp(-r/\xi)$. Such an exponential decay is expected since within the KBdG formalism, a Kondo hole is equivalent to an f-electron state with on-site energy $\varepsilon_f = \infty$. Such a state it localized, and its effects on $\Delta\chi$ or Δs necessarily decay exponentially. With increasing magnetic interaction, ξ increases approximately linearly (see Fig. S2 in the Supplementary Information), leading to a the growth in the spatial extent and amplitude of the perturbations in $\Delta\chi$, as can directly be seen from a comparison of Figs. 1e and 1f. These perturbations are therefore a direct measure for the strength of the magnetic interaction and the resulting correlations in the material.

The spatial perturbations in the electronic correlations, $s(\mathbf{r})$ possess a direct spectroscopic signature in the local density of states of the conduction band, $N_c(\mathbf{r},\omega)$, which can be probed via scanning tunneling spectroscopy (STS)[24–28]. The LDOS describes the quantum mechanical probability to add (for $\omega > 0$) or remove (for $\omega < 0$) a conduction electron with energy $\hbar\omega$ from the system at site $\mathbf{r}$. $N_c(\mathbf{r},\omega)$ for an unperturbed Kondo lattice, shown in Fig. 2a, exhibits a gap which is the primary spectroscopic signature of the hybridization between the conduction band and f-electron state of the magnetic atoms, and the concomitant screening of the magnetic moments. This gap was recently observed for the first time in STS experiments by Schmidt *et al.*[29]. The peak in the LDOS at the low-energy site of the gap arises from the Van Hove singularity of the hybridized Fermi sea (indicated by the green arrow in Fig. 1b). A comparison with the LDOS at the site of the Kondo hole reveals a significant shift of spectral weight from negative to positive energies. To understand this redistribution, we note that the screening of a single Kondo atom by conduction electrons leads to an increase in the local electron density,

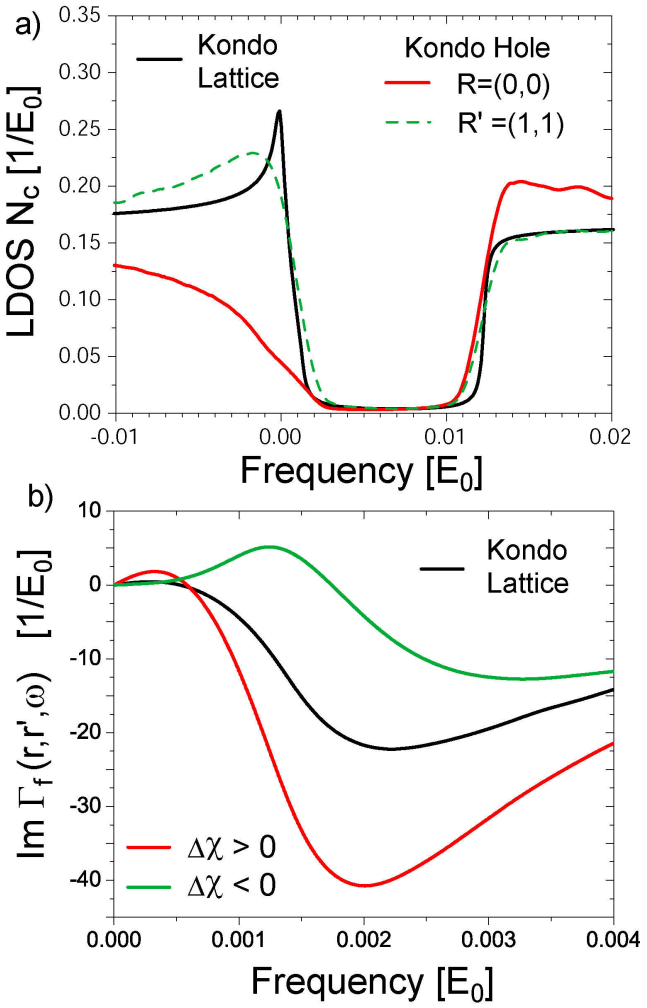

Figure 2: **Spectroscopic Fingerprints a.** The local conduction band density of state $N_c(\mathbf{r},\omega)$ for the unperturbed Kondo lattice, and at the site of the Kondo hole, $\mathbf{R}=(0,0)$, and its next-nearest-neighbor site $\mathbf{R}'=(1,1)$ where $\Delta s(\mathbf{R}')>0$. **b.** The non-local f-electron spin susceptibility, $\Gamma_f(\mathbf{r},\mathbf{r}',\omega)$ between nearest neighbor sites in the unperturbed Kondo lattice, and in the Kondo hole system between sites $\mathbf{r}=(1,1)$ and $\mathbf{r}'=(1,0)$ with $\Delta\chi>0$ and between sites $\mathbf{r}=(1,1)$ and $\mathbf{r}'=(1,2)$ with $\Delta\chi<0$.

$n_c(\mathbf{r})$, which is related to the LDOS via

$$n_c(\mathbf{r}) = \int_{-\infty}^{\infty} d\omega\; n_F(\omega)\; N_c(\mathbf{r},\omega) \qquad (1)$$

with n_F being the Fermi distribution function. An increase in $n_c(\mathbf{r})$ therefore necessarily implies a redistribution of spectral weight in $N_c(\mathbf{r},\omega)$ from positive to negative energies. The removal of a Kondo atom from the lattice simply leads to the opposite effect with a decrease in $n_c(\mathbf{r})$ at the site of the hole, and the corresponding shift in the LDOS shown in Fig. 2a. This suggests that $N_c(\mathbf{r},\omega)$ directly reflects the perturbations in $s(\mathbf{r})$, since for a site with $\Delta s(\mathbf{r})>0$ one has $\Delta n_c(\mathbf{r})>0$, and a concomitant redistribution of spectral weight in $N_c(\mathbf{r},\omega)$ to negative frequencies (and vice versa). Indeed, a plot of $N_c(\mathbf{r},\omega)$ at the next-nearest neighbor site of the Kondo hole, $\mathbf{R}'$, with $\Delta s(\mathbf{R}')>0$, exhibits an increase in the spectral weight at negative frequencies, and hence confirms this conclusion (see Fig. 2a).

The spatial perturbations in the magnetic correlations, $\chi(\mathbf{r},\mathbf{r}')$, possess a spectroscopic signature in the non-local f-electron spin susceptibility, $\Gamma_f(\mathbf{r},\mathbf{r}',\omega)$, between nearest neighbor sites $\mathbf{r}$ and $\mathbf{r}'$. Γ_f can in general be measured via atomic force microscopy[30], and its Fourier transform describes how magnetic correlations decay in real time. A plot of $\mathrm{Im}\Gamma_f(\mathbf{r},\mathbf{r}',\omega)$ in Fig. 2b illustrates the important relation with $\Delta\chi$. In comparison to the unperturbed Kondo lattice, one finds that for two sites $\mathbf{r},\mathbf{r}'$ with $\Delta\chi>0$, $|\mathrm{Im}\Gamma_f|$ is enhanced, while $\Delta\chi<0$ leads to its suppression.

Replacing a Kondo atom by a non-magnetic impurity[20–23] gives rise to a local scattering potential for the conduction electrons (see Sec. S2 of the Supplemental Information). This, in turn, induces perturbations in Δn_c, Δs, and $\Delta\chi$ (see Figs. 3a-c) that possess several distinct differences to those caused by a Kondo hole. In particular, if the non-magnetic scattering potential is attractive, $U_0<0$, the spatial pattern of Δn_c is inverted, i.e., a site with $\Delta n_c>0$ for the Kondo hole case, now has $\Delta n_c<0$ (cf. Figs. 1d and 3a). Since the same inversion occurs for the spatial patterns of Δs and $\Delta\chi$, we conclude that the electronic and magnetic correlations are strongly affected by the spatial redistribution of n_c. Moreover, an *impurity bound state* can be formed around the non-magnetic impurity, whose spectroscopic signature is a sharp peak in $N_c(\mathbf{r},\omega)$ inside the hybridization gap, as shown in Fig. 3d. The emergence of this impurity state is tied to an attractive scattering potential, $U_0<0$, whose magnitude exceeds a critical value, U_c, which is determined by the particle-hole asymmetry of the conduction band. A non-zero U_c could be responsible for the observation that different non-magnetic impurities can lead to disparate properties of the system[20]. With increasing $|U_0|$, the bound state first emerges at the high energy side of the hybridization gap and then moves to lower energies, as shown in Fig. 3d. This bound state is predominantly formed by f-electron states, as can be deduced from a spatial contour plot of $N_c(\mathbf{r},\omega)$ at the bound state energy, Ω_B, shown in Fig. 3e. The bound state is spatially isotropic, and decays exponentially with distance from the non-magnetic impurity with a decay length, $\xi_D\approx 0.65a_0$. If this bound state were formed by (light) conduction electron states, a simple estimate shows that it would possess a decay length in excess of $60a_0$, in disagreement with the results of Fig. 3e. This result is particularly interesting since the non-magnetic impurity leads to scattering in the conduction band only. In contrast, the spatial oscillations of $N_c(\mathbf{r},\omega)$ for frequencies outside the hybridization gap are delocalized,

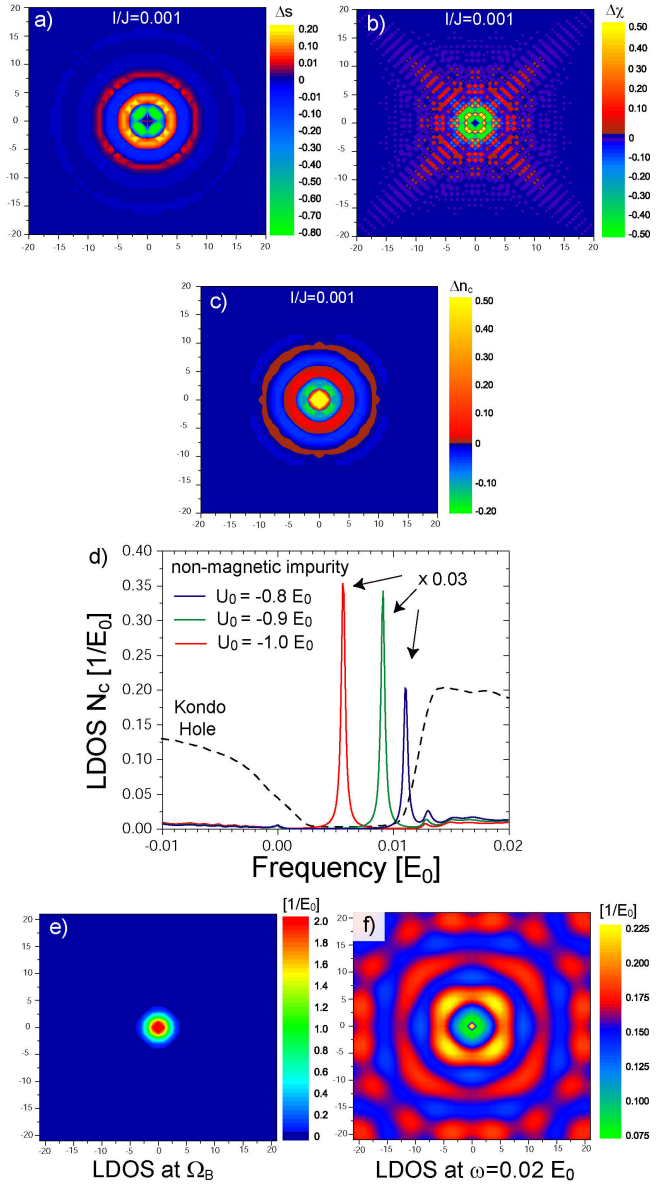

Figure 3: **Local density of states around a defect** Spatial contour plot of **a.** Δs, **b.** $\Delta\chi$, and **c.** Δn_c for a non-magnetic impurity with $U_0 = -1.0E_0$ and $I/J = 0.001$. **d.** Comparison of $N_c(\mathbf{r},\omega)$ at the site of a Kondo hole and of a non-magnetic impurity. An impurity bound state inside the hybridization gap emerges only for an attractive non-magnetic impurity if $|U_0| > U_c = 0.62E_0$. To facilitate the comparison, the curves of the bound state have been multiplied by 0.03. Spatial contour plot of $N_c(\mathbf{r},\omega)$ for $U_0 = -1.0E_0$ at **e.** the energy of the bound state, $\omega = \Omega_B$, and **f.** outside the hybridization gap at $\omega = 0.02E_0$.

as exemplified in Fig. 3f, and hence are predominantly arising from the (light) conduction electron band.

The strongly correlated nature of the Kondo lattice also manifests itself in highly non-linear quantum interference of the spatial perturbations in χ and s emanating from adjacent Kondo holes. In a periodic

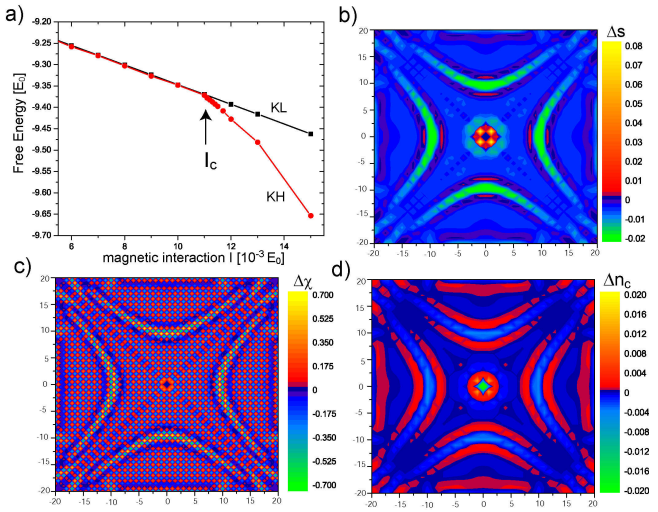

Figure 4: **Novel Ground State driven by Quantum Interference** Periodic array of Kondo holes: **a.** Free energy for an unperturbed Kondo lattice (KL) and a Kondo hole (KH) array as a function of I/J. For the electronic band structure considered here, one has $I_c/J = 0.0011(1)$, indicated by an arrow. Contour plots of **b.** Δs, **c.** $\Delta\chi$, and (**d.** Δn_c for $I/J = 0.0013 > I_c/J$.

array of Kondo holes, this non-linearity drives the system to a novel inhomogeneous ground state via a first order phase transition once I exceeds a critical value, I_c, as demonstrated by a plot of the free energy in Fig. 4a. Note that I_c increases with increasing distance between the Kondo holes. This novel inhomogeneous ground state is characterized by spatial patterns of $\Delta\chi$, Δs, and Δn_c [see Figs. 4b-d], that are strikingly different from the ones for $I < I_c$ shown in Fig. 1. The similarity of these three spatial patterns, as well as the significant amplitude of the perturbations in the conduction electron density, n_c, suggest that while the phase transition is driven by quantum interference of the correlations' spatial perturbations, the resulting real space patterns are determined by the redistributed conduction electron density. Changing the symmetry of periodic array, for example, by adding a second hole to the unit cell (see Fig. S3 of the Supplemental Information), leads to a significant change in the spatial pattern for $I > I_c$, reflecting the strong non-linearity of the system.

We would like to thank E. Abrahams, P. Coleman, J.C. Davis, H. Manoharan, S. Sachdev, Q. Si, F. Steglich and H. v. Lohneysen for stimulating discussions. D.K.M. would like to thank the Aspen Center for Physics and the James Franck Institute at the University of Chicago for its hospitality during various stages of this project. This work is supported by the U.S. Department of Energy under Award No. DE-FG02-05ER46225.

[1] Doniach, S. The Kondo lattice and weak antiferromagnetism. *Physica B* **91**, 231 (1977).

[2] Kondo, J. Resistance minimum in dilute magnetic alloys. *Prog. Theor. Phys.* **32**, 37-49 (1964).

[3] Maple, M.B., *et al.*, Non-fermi-Liquid ground states in strongly correlated f-electron materials, *J. Low Temp. Phys.* **99**, 223 (1995).

[4] Schroder, A. *et al.* Onset of antiferromagnetism in heavy-fermion metals. *Nature (London)* **407**, 351 (2000).

[5] Stewart, G.R. Non-Fermi-liquid behavior in d- and f-electron metals. *Rev. Mod. Phys.* **73**, 797 (2001).

[6] Custers, J. *et al.* The break-up of heavy electrons at a quantum critical point. *Nature* **424**, 524 (2003).

[7] von Lohneysen, H., Rosch, A., Vojta, M. & Woelfle, P. Fermi-liquid instabilities at magnetic quantum phase transitions. *Rev. Mod. Phys.* **79**, 1015 (2007).

[8] Gegenwart, P., Si, Q., & Steglich, F. Quantum criticality in heavy-fermion metals. *Nature Physics*, **4**, 186 (2008).

[9] Balatsky, A.V., Vekhter, I. & Zhu, J.X. Impurity-induced states in conventional and unconventional superconductors. *Rev. Mod. Phys.* **78**, 373 (2006).

[10] Yazdani, A., Howald, C.M., Lutz, C.P., Kapitulnik, A. & Eigler, D.M. Impurity-induced bound excitations on the surface of $Bi_2Sr_2CaCu_2O_8$. *Phys. Rev. Lett.* **83**, 176 (1999).

[11] Hudson, E.W., Pan, S.H., Gupta, A.K., Ng, K.W. & Davis, J.C. Atomic-scale quasi-particle scattering resonances in $Bi_2Sr_2CaCu_2O_{8+\delta}$. *Science* **285**, 88 (1999).

[12] Hudson, E.W. *et al.* Interplay of magnetism and high-T_c superconductivity at individual Ni impurity atoms in $Bi_2Sr_2CaCu_2O_{8+\delta}$. *Nature (London)* **411**, 920 (2001).

[13] Hewson, A.C. The Kondo Problem to Heavy Fermions *(Cambridge University Press, Cambridge, 1993).*

[14] Fulde, P., Keller, J. & Zwicknagl, G. Theory of heavy fermion systems. *Sol. Stat. Phys.* **41**, 1 (1988).

[15] Coleman, P., Pepin, C., Si, Q., & Ramazashvili, R. How do Fermi liquids get heavy and die? *J. Phys. Cond. Mat.* **13**, R723 (2001).

[16] Si, Q.M., Rabello, S., Ingersent, K. & Smith, J.L. Locally critical quantum phase transitions in strongly correlated metals. *Nature* **413**, 804 (2001).

[17] Sun, P. & Kotliar, G. Extended dynamical mean field theory study of the periodic Anderson model. *Phys. Rev. Lett.* **91**, 037209 (2003).

[18] Senthil, T., Sachdev, S. & Vojta, M. Fractionalized Fermi liquids. *Phys. Rev. Lett.* **90**, 216403 (2003).

[19] Paul, I., Pepin, C. & Norman, M.R. Kondo breakdown and hybridization fluctuations in the Kondo-Heisenberg lattice. *Phys. Rev. Lett.* **98**, 026402 (2007).

[20] Steglich, F., Ahlheim, U, Rauchschwalbe, U. & Spille, H. Heavy Fermions and Superconductivity: "Superconducting Spectroscopy" of non-magnetic impuities in $CeCu_2Si_2$. *Physica B* **148**, 6 (1987).

[21] Lin, C.L., Wallash, A., Crow, J.E., Mihalisin, T. & Schlottmann, P. Heavy-Fermion Behavior and the Single-Ion Kondo Model. *Phys. Rev. Lett.* **58**, 1232 (1987).

[22] Lopez de la Torre, A. et al. Th-doped URu_2Si_2: influence of Kondo holes on coexisting superconductivity and magnetism. *Physica B, 179*, 208-214 (1992).

[23] Lawrence, J.M. *et al.*, Kondo hole behavior in $Ce_{0.97}La_{0.03}Pd_3$. *Phys. Rev. B* **53**, 12559 (1996).

[24] Li, J., Schneider, W.-D., Berndt, R. & Delley, B. Kondo Scattering Observed at a Single Magnetic Impurity. *Phys. Rev. Lett.* **80**, 2893 (1998).

[25] Ujsaghy O, Kroha J, Szunyogh L, Zawadowski A. Theory of the Fano resonance in the STM tunneling density of states due to a single Kondo impurity. *Phys. Rev. Lett.* **85**, 2557 (2000).

[26] Madhavan, V., Chen, W., Jamneala, T., Crommie, M.F. & Wingreen N.S. Local spectroscopy of a Kondo impurity: Co on Au(111). *Phys. Rev. B* **64**, 165412 (2001).

[27] Maltseva, M., Dzero, M. & Coleman, P. Electron Cotunneling into a Kondo Lattice. *Phys. Rev. Lett.* **103**, 206402 (2009).

[28] Figgins, J. & Morr, D. K. dI/dV and Quantum Interference in Kondo Systems, preprint.

[29] Schmidt, A.R. *et al.* Emergence of the 'Hidden Order' state from the 'Fano Lattice' electronic structure of the heavy-fermion material URu_2Si_2. preprint, submitted.

[30] Hammel, P.C. Seeing single spins, *Nature* **430**, 300 (2004).

Supplemental Online Information for

Defects in Heavy-Fermion Materials:
Unveiling Strong Correlations in Real Space

by Jeremy Figgins and Dirk K. Morr

Section S1: Supplemental Figures

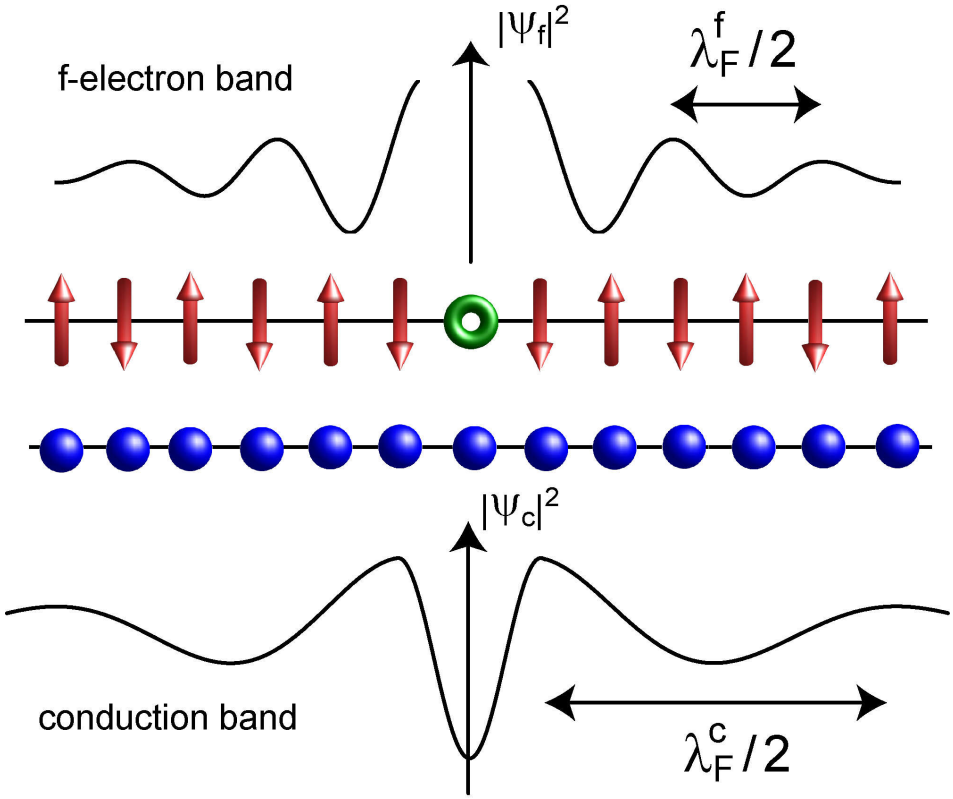

Figure 1: **Defect in a Kondo lattice** Blue dots represent the sites of the metallic conduction lattice, while red arrows show the locations of the magnetic moments, i.e., the magnetic Kondo atoms, in the Kondo lattice. The green ring denotes the site of a missing Kondo atom, i.e., a Kondo hole, or of a non-magnetic impurity, where the latter leads to scattering of the conduction electrons only. The defect induces spatial perturbations in the electronic and magnetic correlations of the system, which are determined by the real space oscillations of $|\Psi_c|^2$ with wavelength $\lambda_F^c/2$ and $|\Psi_f|^2$ with wavelength $\lambda_F^f/2$. Here, Ψ_c and Ψ_f are the wave functions of the conduction and f-electron states, respectively, with λ_F^c and λ_F^f being their associated Fermi wavelengths.

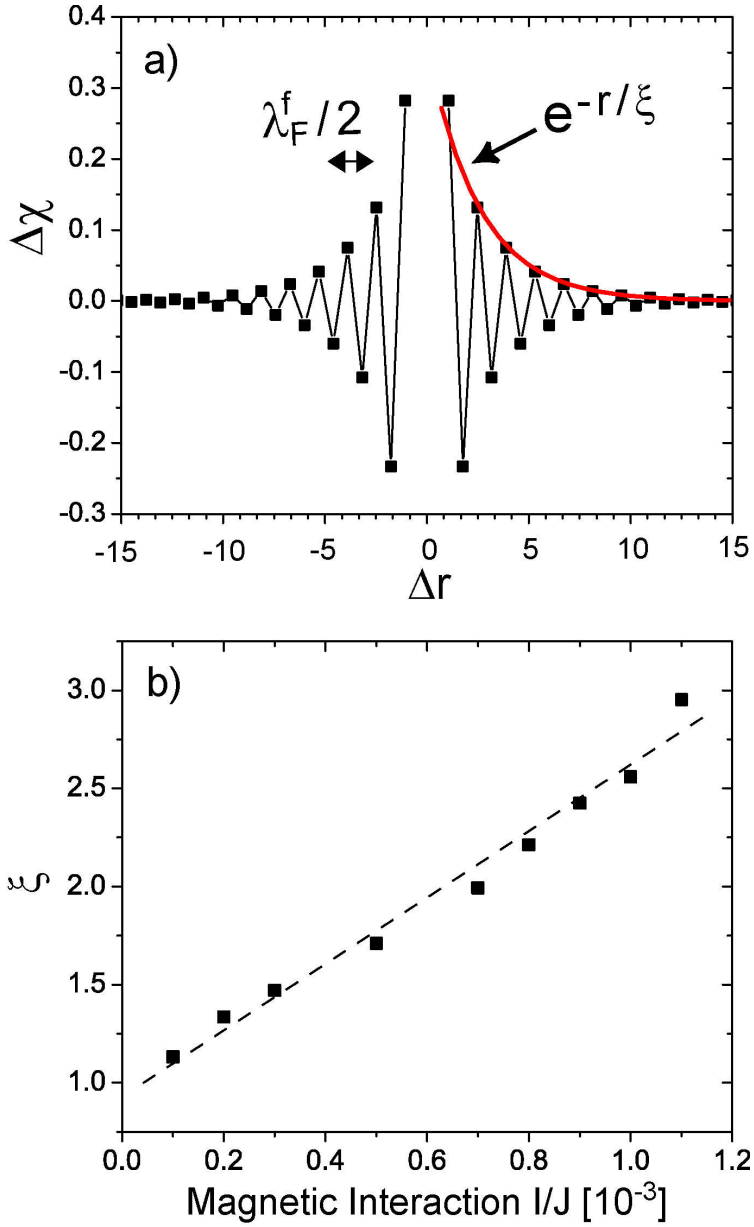

Figure 2: **Spacial oscillations of** $\Delta\chi$ a) Spatial oscillations of $\Delta\chi(\mathbf{r},\mathbf{r}')$ (shown as a function of $\Delta r = |\mathbf{r}+\mathbf{r}'|/2$ measured from the Kondo hole) along the lattice diagonal. The oscillations exhibit a wavelength $\lambda_F^f/2$ and decay exponentially as $e^{-r/\xi}$ (the exponential fit is shown as a red line). b) Dependence of ξ on the magnetic interaction, I. Errors in ξ are smaller than the data points. ξ increases approximately linearly with I/J (dashed line is a guide to the eye).

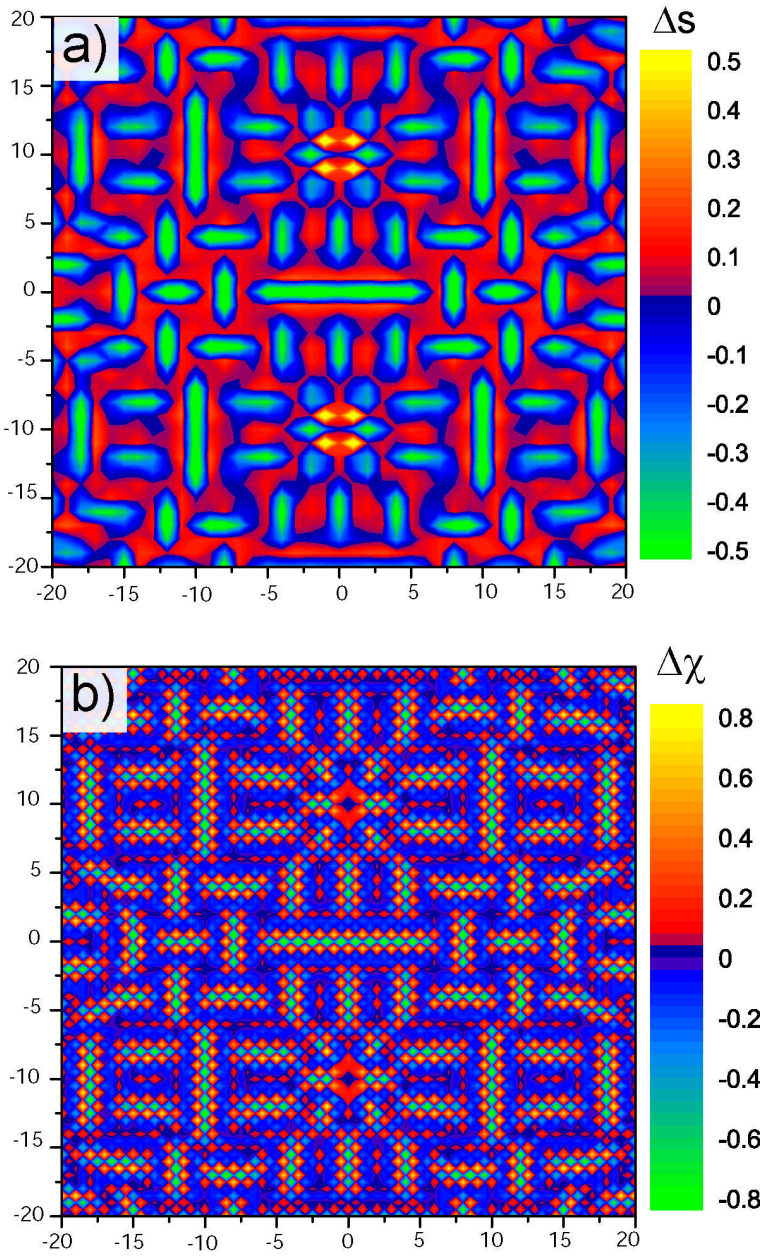

Figure 3: **Quantum Interference in a periodic array of Kondo holes with two Kondo holes per unit cell** Contour plot of (a) Δs and (b) $\Delta\chi$ for $I/J = 0.0013 > I_c/J$. The spatial interference pattern for $I > I_c$ is distinctively different from that of a periodic array with a single Kondo hole per unit cell (shown in Fig. 4), reflecting the strong non-linearity of the system.

Section S2: The Kondo-Bogoliubov-de Gennes (KBdG) Formalism

Starting point for the study of defects in Kondo lattice systems is the Kondo Heisenberg Hamiltonian

$$\mathcal{H} = -\sum_{\mathbf{r},\mathbf{r}',\sigma} t_{\mathbf{r},\mathbf{r}'} c^{\dagger}_{\mathbf{r},\sigma} c_{\mathbf{r}',\sigma} + J{\sum_{\mathbf{r}}}' \mathbf{S}^K_{\mathbf{r}} \cdot \mathbf{s}^c_{\mathbf{r}} + {\sum_{\mathbf{r},\mathbf{r}'}}' I_{\mathbf{r},\mathbf{r}'} \mathbf{S}^K_{\mathbf{r}} \cdot \mathbf{S}^K_{\mathbf{r}'} \ , \tag{S1}$$

where $t_{\mathbf{r},\mathbf{r}'}$ is the fermionic hopping element between sites $\mathbf{r}$ and $\mathbf{r}'$, and $c^{\dagger}_{\mathbf{r},\sigma}, c_{\mathbf{r},\sigma}$ creates (annihilates) a conduction electron with spin σ at site $\mathbf{r}$. $J > 0$ is the Kondo coupling, and $\mathbf{S}^K_{\mathbf{r}}$ and $\mathbf{s}^c_{\mathbf{r}}$ are the $S = 1/2$ spin operators of the magnetic (Kondo) atom and the conduction electron at site $\mathbf{r}$, respectively. $I_{\mathbf{r},\mathbf{r}'} > 0$ is the antiferromagnetic interaction between Kondo atoms at sites $\mathbf{r}$ and $\mathbf{r}'$, which we restrict to nearest-neighbor sites below. We take the lattices of the conduction band and that of the magnetic (Kondo) atoms to possess identical structures and lattice constants. Thus, the site of a Kondo atom and the (single) conduction site that it couples to are denoted by the same $\mathbf{r}$. The unprimed sum runs over all sites of the conduction lattice, while the primed sum runs over all positions of the Kondo atoms. These two sums are identical for an unperturbed Kondo lattice without any defects.

A systematic large-N expansion[1–9] of the Hamiltonian can be achieved by generalizing the spin operators to $SU(N)$ and representing them using Abrikosov pseudofermions

$$\mathbf{S}^K_{\mathbf{r}} = \sum_{\alpha,\beta} f^{\dagger}_{\mathbf{r},\alpha} \boldsymbol{\sigma}_{\alpha,\beta} f_{\mathbf{r},\beta} \quad \mathbf{s}^c_{\mathbf{r}} = \sum_{\alpha,\beta} c^{\dagger}_{\mathbf{r},\alpha} \boldsymbol{\sigma}_{\alpha,\beta} c_{\mathbf{r},\beta} \ , \tag{S2}$$

where $\alpha, \beta = 1, ..., N$ and $\boldsymbol{\sigma}_{\alpha,\beta}$ are the generators of $SU(N)$. Here, $f^{\dagger}_{\mathbf{r},\alpha}$ ($f_{\mathbf{r},\alpha}$) creates a pseudofermion in the f-electron state of the magnetic Kondo atom. In addition, one needs to satisfy the constraint that each magnetic atom (i.e., each f-electron site) is occupied by $N/2$ particles, i.e.,

$$\hat{n}_f(\mathbf{r}) = \sum_{\alpha} f^{\dagger}_{\mathbf{r},\alpha} f_{\mathbf{r},\alpha} = \frac{N}{2} \ . \tag{S3}$$

Inserting the representations of Eq.(S2) into the Hamiltonian,Eq.(S1), yields quartic fermionic interaction terms. Since our objective is the study of Kondo lattices containing defects which break the translational invariance, it is necessary to introduce a mean-field decoupling of the resulting interaction terms in real space. The mean-field theory of the homogeneous Kondo lattice (or the single Kondo impurity) becomes exact in the limit $N \to \infty$[1,2]. However, it was argued that even for $N = 2$, the qualitative and to a large extent quantitative features of the mean-field solutions remain unchanged[4,9], which in certain limits has been validated by the comparison with exact numerical renormalization group studies[10]. Following this argument, we set $N = 2$ below, and introduce the following local and non-local expectation values

$$s(\mathbf{r}) = \frac{J}{2} \sum_{\alpha} \langle f^{\dagger}_{\mathbf{r},\alpha} c_{\mathbf{r},\alpha} \rangle \, ; \quad \chi(\mathbf{r},\mathbf{r}') = \frac{I_{\mathbf{r},\mathbf{r}'}}{2} \sum_{\alpha} \langle f^{\dagger}_{\mathbf{r},\alpha} f_{\mathbf{r}',\alpha} \rangle \ . \tag{S4}$$

Here, $s(\mathbf{r})$ describes the local hybridization between the conduction electron states and the magnetic f-electron states, whose magnitude is a measure of the Kondo screening. Thus $s(\mathbf{r}) = 0$ represents an unscreened magnetic moment at site $\mathbf{r}$. $\chi(\mathbf{r},\mathbf{r}')$ is a measure of the magnetic correlations between Kondo atoms[7,9]. To enforce the constraint $\langle \hat{n}_f(\mathbf{r}) \rangle = 1$ within our formalism, we add the term $\sum_{\mathbf{r},\alpha} \varepsilon_f(\mathbf{r}) f^{\dagger}_{\mathbf{r},\alpha} f_{\mathbf{r},\alpha}$ to the Hamiltonian in Eq.(S1), where $\varepsilon_f(\mathbf{r})$ represents the on-site energy of the f-electrons. The resulting Hamiltonian is quadratic, containing the set of parameters $\{s(\mathbf{r}), \chi(\mathbf{r},\mathbf{r}'), \varepsilon_f(\mathbf{r})\}$, and therefore can be diagonalized in real space (we assume periodic boundary conditions). After each diagonalization, the mean-fields $s(\mathbf{r})$ and $\chi(\mathbf{r},\mathbf{r}')$ are computed self-consistently via Eq.(S4), and $\varepsilon_f(\mathbf{r})$ is chosen such that $\langle \hat{n}_f(\mathbf{r}) \rangle = 1$ at each site. This procedure is repeated until a self-consistent solution for $\{s(\mathbf{r}), \chi(\mathbf{r},\mathbf{r}'), \varepsilon_f(\mathbf{r})\}$ is obtained. We note that for an unperturbed Kondo lattice, this formalism is identical to the saddle-point approximation of the path-integral approach[1].

In order to describe a Kondo hole at site $\mathbf{R}$, we remove the corresponding spin operator, $\mathbf{S}^K_{\mathbf{R}}$ from the Hamiltonian in Eq.(S1)[8]. When a Kondo atom at site $\mathbf{R}$ is replaced by a non-magnetic impurity, the spin operator $\mathbf{S}^K_{\mathbf{R}}$ is removed, and the term $U_0 \sum_{\alpha} c^{\dagger}_{\mathbf{R},\alpha} c_{\mathbf{R},\alpha}$ is added to the Hamiltonian, where U_0 is the non-magnetic scattering strength. Here, we assume that the non-magnetic atom leads to scattering of the conduction electrons only, since the magnetic f-electron states are not expected to hybridize with the electronic states of the non-magnetic impurity, in agreement with Ref. 11, but in contrast to Ref. 12.

For the results shown in the article, we took the conduction and Kondo lattices to be finite two-dimensional square lattices containing each $\mathcal{N} = M \times M$ sites. Our formalism can equally well be applied to three-dimensional lattices, however, we do not expect that the qualitative nature of the results shown in this article will be changed. For the conduction band, we employ a nearest-neighbor hopping, $t = 0.5E_0$, and a chemical potential, $\mu = -1.809E_0$. Here, E_0 is an overall energy scale related to the conduction bandwidth $W = 4E_0$. These parameters yield an isotropic conduction Fermi surface (see Fig. 1b) with Fermi-wave-length $\lambda_F^c = 10a_0$, where a_0 is the lattice constant, and a band filling (per spin degree) of $\pi/100$.

We choose the size of the lattice sufficiently large such that the set of solutions for $\{s(\mathbf{r}), \chi(\mathbf{r}, \mathbf{r}'), \varepsilon_f(\mathbf{r})\}$ is independent of $\mathcal{N}$. The results shown in the main text were obtained for systems with $M = 41$, and we did not find any significant quantitative changes for lattice sizes up to $M = 71$. For the unperturbed Kondo lattices with $J = 1.0E_0$, the set of parameters for several values of I/J are shown in Table 1.

I/J	ε_f	s	χ
0.0005	0.001247	0.048470	0.00008122
0.001	0.001232	0.048470	0.00016579
0.0011	0.001229	0.048470	0.00018281
0.0013	0.001225	0.048470	0.00021688

Table I: Values for s, χ, and ε_f (in units of E_0) for an unperturbed Kondo lattice as a function of I/J. Note that for these small values of I/J, s remains practically unchanged. A significant reduction of s is only seen for larger values of I/J.

Section S3: The Local Density of States of the Conduction Band

In general, the local density of state for the conduction band, $N_c(\mathbf{r}, \omega)$, can be directly obtained from the eigenvectors and energies of the diagonalization procedure described in the previous section. However, the finite size of the systems leads to (artifactual) strong oscillations in the frequency dependence of the LDOS. We developed an alternative approach to circumvent this problem, and verified that it significantly reduces the artifactual frequency oscillations, and that it yields identical results to the first approach when considering the spatial form of $N_c(\mathbf{r}, \omega)$ at fixed ω. In this approach, we compute the local conduction electron density of states at a site $\mathbf{r}$ for a given set of solutions, $\{s(\mathbf{r}), \chi(\mathbf{r}, \mathbf{r}'), \varepsilon_f(\mathbf{r})\}$ via

$$N_c(\mathbf{r}, \omega) = -\frac{1}{\pi}\mathrm{Im}[G(\mathbf{r}, \mathbf{r}, \omega)] \ , \tag{S5}$$

where $G(\mathbf{r}, \mathbf{r}, \omega)$ is the full retarded conduction band Green's function given by (in what follows, all Greens functions are retarded)

$$G(\mathbf{r}, \mathbf{r}, \omega) = G_0(\mathbf{r}, \mathbf{r}, \omega) + \hat{G}_0^{(1)}(\Delta\mathbf{r}, \omega)\hat{s}\hat{F}(\omega)\hat{s}\hat{G}_0^{(2)}(-\Delta\mathbf{r}, \omega) \ . \tag{S6}$$

Here we defined

$$\hat{G}_0^{(1)}(\Delta\mathbf{r}, \omega) = (G_0(\mathbf{r}, \mathbf{r}_1, \omega), ..., G_0(\mathbf{r}, \mathbf{r}_\mathcal{P}, \omega)) \ ; \quad \hat{G}_0^{(2)}(-\Delta\mathbf{r}, \omega) = \begin{pmatrix} G_0(\mathbf{r}_1, \mathbf{r}, \omega) \\ \vdots \\ G_0(\mathbf{r}_\mathcal{P}, \mathbf{r}, \omega) \end{pmatrix} \ , \tag{S7}$$

where G_0 is the Greens function of the decoupled (unhybridized) conduction band, $\mathbf{r}_i$ is the position of the $i'th$ Kondo

atom, and $\mathcal{P}$ is the number of Kondo atoms in the system. Moreover, for the hybridization matrix $\hat{s}$ one has

$$\hat{s} = \begin{pmatrix} s(\mathbf{r}_1) & 0 & 0 & 0 & 0 \\ 0 & s(\mathbf{r}_2) & 0 & 0 & 0 \\ 0 & 0 & ... & 0 & 0 \\ 0 & 0 & 0 & s(\mathbf{r}_{\mathcal{P}-1}) & 0 \\ 0 & 0 & 0 & 0 & s(\mathbf{r}_{\mathcal{P}}) \end{pmatrix} , \tag{S8}$$

and $\hat{F}$ is the full f-electron Green's function with the (ij) element of its inverse given by

$$\left[\hat{F}(\omega)^{-1}\right]_{ij} = \begin{cases} \omega - \varepsilon_f(\mathbf{r}_i) - s(\mathbf{r}_i)G_0(\mathbf{r}_i, \mathbf{r}_j, \omega)s(\mathbf{r}_j) & \text{if } i = j \\ \chi(\mathbf{r}_i, \mathbf{r}_j) - s(\mathbf{r}_i)G_0(\mathbf{r}_i, \mathbf{r}_j, \omega)s(\mathbf{r}_j) & \text{if } i \neq j \ . \end{cases} \tag{S9}$$

In the presence of a non-magnetic impurity scatterer at site $\mathbf{R}$ with potential U_0, it is easy to show that the full conduction electron Green's function can be obtained from

$$G_{NM}(\mathbf{r}, \mathbf{r}, \omega) = G(\mathbf{r}, \mathbf{r}, \omega) + \frac{G(\mathbf{r}, \mathbf{R}, \omega)U_0 G(\mathbf{R}, \mathbf{r}, \omega)}{1 - U_0 G(\mathbf{R}, \mathbf{R}, \omega)} \tag{S10}$$

with $G(\mathbf{r}, \mathbf{r}', \omega)$ obtained from Eq.(S6).

Section S4: The f-electron Spin Susceptibility

The f-electron spin susceptibility, Γ_f, in Matsubara time is given by

$$\Gamma_f(\mathbf{r}, \mathbf{r}', \tau) = \langle T_\tau \mathbf{S}^K_{\mathbf{r}}(\tau) \cdot \mathbf{S}^K_{\mathbf{r}'}(0) \rangle \ . \tag{S11}$$

After Fourier transformation into Matsubara frequency space, and analytic continuation, one obtains ($k_B = 1$)

$$\Gamma_f(\mathbf{r}, \mathbf{r}', i\Omega_m) = \frac{3}{2} T \sum_n F(\mathbf{r}, \mathbf{r}', i\omega_n) F(\mathbf{r}', \mathbf{r}, i\omega_n + i\Omega_m) \ , \tag{S12}$$

where F is the f-electron Greens functions from Eq.(S9). Using next the Lehmann representation of F, one obtains for the imaginary part of the retarded f-electron spin susceptibility

$$\mathrm{Im}\,\Gamma_f(\mathbf{r}, \mathbf{r}', \Omega) = \frac{3}{2\pi} \int_0^\Omega d\upsilon \, \mathrm{Im}F(\mathbf{r}, \mathbf{r}', \upsilon) \, \mathrm{Im}F(\mathbf{r}', \mathbf{r}, \upsilon - \Omega) \ . \tag{S13}$$

[1] Coleman, P. 1/N expansion for the Kondo lattice, *Phys. Rev. B* **28**, 5255 (1983).
[2] Read, N. & Newns, D.M. On the solution of the Coqblin-Schreier Hamiltonian by the large-N expansion technique, *J. Phys. C* **16**, 3273 (1983).
[3] Millis, A.J. & Lee, P.A. Large-orbital-degeneracy expansion for the lattice Anderson model. *Phys. Rev. B* **35**, 3394 (1987).
[4] Bickers, N.E. Review of techniques in the large-N expansion for dilute magnetic alloys. *Rev. Mod. Phys.* **59**, 845 (1987).
[5] Affleck, I. & Marston, B. Large-n limit of the Heisenberg-Hubbard model: Implications for the high-T_c cuprates. *Phys. Rev. B* **37**, 3774 (1988).
[6] Hewson, A.C. The Kondo Problem to Heavy Fermions *(Cambridge University Press, Cambridge, England, 1993)*.
[7] Senthil, T., Vojta, M. & Sachdev, S. Weak magnetism and non-Fermi liquids near heavy- fermion critical points. *Phys. Rev. B* **69**, 035111 (2004).
[8] Kaul, R. K. & Vojta, M. Strongly inhomogeneous phases and non-Fermi-liquid behavior in randomly depleted Kondo lattices. *Phys. Rev. B* **75**, 132407 (2007).
[9] Paul, I., Pepin, C. & Norman, M.R. Kondo breakdown and hybridization fluctuations in the Kondo-Heisenberg lattice. *Phys. Rev. Lett.* **98**, 026402 (2007).
[10] Silva, J.B., Lima, W.L.C., Oliveira, W.C., Mello, J.L.N., Oliveira, L.N. & Wilkins, J.W. Particle-Hole Asymmetry in the Two-Impurity Kondo Model. **Phys. Rev. Lett. 76**, 275 (1996).
[11] Freytag, R. & Keller, J. Dynamical conductivity of heavy fermion systems: effect of impurity scattering. *Z. Phys. B - Condensed Matter* **80**,241 (1990).
[12] Sollie, R. & and Schlottmann, P. A simple theory of the Kondo Hole. *J.Appl. Phys.* **69**, 5478 (1991).